Vibrio cholerae filamentation promotes chitin surface attachment at the expense of competition in biofilms

Benjamin R. Wucher[a], Thomas M. Bartlett[b], Mona Hoyos[c], Kai Papenfort[c], Alexandre Persat[d,e], and Carey D. Nadell[a,1]

[a]Department of Biological Sciences, Dartmouth College, Hanover, NH 03755; [b]Department of Microbiology, Harvard Medical School, Boston, MA 02115; [c]Department of Microbiology, Faculty of Biology I, Ludwig Maximilians University of Munich, 82152 Martinsried, Germany; [d]Institute of Bioengineering, School of Life Sciences, École Polytechnique Fédérale de Lausanne, 1015 Lausanne, Switzerland; and [e]Global Health Institute, School of Life Sciences, École Polytechnique Fédérale de Lausanne, 1015 Lausanne, Switzerland

Edited by Thomas J. Silhavy, Princeton University, Princeton, NJ, and approved June 3, 2019 (received for review November 13, 2018)

Collective behavior in spatially structured groups, or biofilms, is the norm among microbes in their natural environments. Though biofilm formation has been studied for decades, tracing the mechanistic and ecological links between individual cell morphologies and the emergent features of cell groups is still in its infancy. Here we use single-cell–resolution confocal microscopy to explore biofilms of the human pathogen *Vibrio cholerae* in conditions mimicking its marine habitat. Prior reports have noted the occurrence of cellular filamentation in *V. cholerae*, with variable propensity to filament among both toxigenic and nontoxigenic strains. Using a filamenting strain of *V. cholerae* O139, we show that cells with this morphotype gain a profound competitive advantage in colonizing and spreading on particles of chitin, the material many marine *Vibrio* species depend on for growth in seawater. Furthermore, filamentous cells can produce biofilms that are independent of primary secreted components of the *V. cholerae* biofilm matrix; instead, filamentous biofilm architectural strength appears to derive at least in part from the entangled mesh of cells themselves. The advantage gained by filamentous cells in early chitin colonization and growth is countered in long-term competition experiments with matrix-secreting *V. cholerae* variants, whose densely packed biofilm structures displace competitors from surfaces. Overall, our results reveal an alternative mode of biofilm architecture that is dependent on filamentous cell morphology and advantageous in environments with rapid chitin particle turnover. This insight provides an environmentally relevant example of how cell morphology can impact bacterial fitness.

Vibrio cholerae | biofilm | extracellular matrix | cell shape | chitin

Bacterial existence in the wild is predominated by life in spatially structured groups, termed biofilms (1), which inhabit environments including the rhizosphere (2), sites of acute and chronic infection (3, 4), pipes of industrial and wastewater flow systems (5), and surfaces of marine snow (6–10). Although living in groups correlates with increased tolerance to exogenous threats like antibiotic exposure (11), biofilm-dwelling cells also experience intense competition for space and resources (12). Furthermore, cells in mature biofilms are generally nonmotile and incur a tradeoff between optimizing local competition versus dispersal to new environments (13–15). Balancing colonization, local growth, and dispersal is therefore a critical element of microbial fitness during biofilm formation, and understanding how bacteria modulate this balance is a central challenge in microbial ecology. Here, we study how variation in individual cell morphology impacts biofilm architecture and the competition/colonization tradeoff among variants of *Vibrio cholerae*.

V. cholerae is a notorious human pathogen responsible for the diarrheal disease cholera, but between epidemics it persists as a common component of aquatic ecosystems, where it consumes chitin harvested from the exoskeletons of arthropods (16, 17). To utilize this resource, *V. cholerae* must colonize and produce biofilms on chitin particles, creating a dense, resource-limited, and architecturally complex space for both interspecies and interstrain competition (18, 19). *V. cholerae* strains that are better adapted to colonize chitin surfaces, exploit the resources embedded in them, and spread to other particles are thus likely to be more frequently represented in estuarine conditions (20, 21). The marine natural history of *V. cholerae* makes this bacterium an ideal candidate for studying the effects of different surface-occupation strategies that might occur in estuarine and oceanic environments (16, 18, 20, 22, 23).

Many strains of *V. cholerae* and other *Vibrio* spp. can be found in the marine environment, with varying propensities for biofilm formation (16, 21). Recent work from several groups has characterized the spatial and temporal patterns of biofilm development in remarkable detail for model strains of *V. cholerae* O1 El Tor, the predominant agent of the modern cholera pandemic. These studies have revealed the localization of different polysaccharide and protein subcomponents of the secreted matrix (24–29), the key cell group architecture transitions and origins of cell–cell orientation (30, 31), and the cell–cell interaction mechanics underlying collective structure in response to fluid flow (32). *V. cholerae* cellular morphology has been carefully studied in laboratory conditions (33–35); however, the degree of *V. cholerae* morphological variation in the environment, the impact of cell shape on biofilm architecture, and the consequences for interstrain competition are less well understood. To explore these questions, we developed a microfluidic assay in which chitin particles are embedded in flow devices perfused with

Significance

The human pathogen *Vibrio cholerae*, when not inside of a host, grows in cell clusters (biofilms) on pieces of detritus in aquatic environments. Here we discovered that some isolates of *V. cholerae* can change their shape from small comma-shaped cells to long filaments in seawater. This altered cell shape allows cells to make new types of biofilms, and provides an advantage in quickly colonizing particles in seawater, at the expense of longer-term competitive ability. The filamentous cell-shape strategy is particularly effective at competing in environments with quick turnover of chitin particles. This result showcases how bacterial cell shape can be coupled to environmental success during surface occupation, competition within biofilms, and dispersal to new resource patches.

Author contributions: B.R.W., T.M.B., A.P., and C.D.N. designed research; B.R.W. performed research; B.R.W., T.M.B., M.H., K.P., A.P., and C.D.N. analyzed data; and B.R.W. and C.D.N. wrote the paper with input from T.M.B, M.H., K.P., and A.P.

The authors declare no conflict of interest.

This article is a PNAS Direct Submission.

Data deposition: The sequences reported in this paper are publicly available at the European Nucleotide Archive (https://www.ebi.ac.uk/ena) under accession nos. ERX3347601–ERX3347606.

[1]To whom correspondence may be addressed. Email: carey.d.nadell@dartmouth.edu.

This article contains supporting information online at www.pnas.org/lookup/suppl/doi:10.1073/pnas.1819016116/-/DCSupplemental.

Published online June 25, 2019.

artificial seawater and onto which cells could be readily inoculated to monitor colonization and biofilm growth.

Surveying samples of *V. cholerae* pandemic isolates from the two major extant serogroups, O1 El Tor and O139, we observed that some variants produce subpopulations of filamented cells under nutrient-limited conditions, including on particles of chitin in seawater. We show that filamentation confers markedly altered chitin colonization and biofilm architecture relative to shorter cells. Differences in chitin colonization and biofilm architecture, in turn, influence competition for space and resources, suggesting that normal-length and filamentous morphotypes are advantageous in different regimes of chitin particle turnover in the water column. Overall, our results highlight a novel mode of biofilm assembly and yield new insights into the potential roles of bacterial filamentation in microbial ecology.

Results

Filamentation in Conditions Mimicking a Marine Habitat. Using simple microfluidic devices in which cells grow on glass substrata under the flow of M9 minimal media, we first explored the cell shape and biofilm architecture of different isolates of *V. cholerae* from the two pandemic serogroups O1 El Tor and O139 (for a full strain list, see *SI Appendix*, Table S1). At least one representative from both serogroups produces subpopulations of filamentous cells in minimal media, and we sought to isolate this morphotype to further understand its consequences for growth and biofilm development. *V. cholerae* AI-1837 from the O139 serogroup and its avirulent derivative, CVD112 (36), filament especially aggressively (*SI Appendix*, Figs. S1 and S5), and we therefore took CVD112 as a model to explore the consequences of filamentation for biofilm growth dynamics. For comparison throughout the study, we use the model strain N16961 (serogroup O1, El Tor biotype), which did not produce filaments under any conditions tested. To allow for visualization of these strains via confocal microscopy, the far-red fluorescent protein-encoding locus *mKate2* was inserted in single copy under the control of a strong constitutive promoter into the chromosomal *lacZ* locus of CVD112 and its derivatives. Analogously, a construct encoding the orange fluorescent protein *mKO-κ* was inserted into the chromosomal *lacZ* of N16961 and its derivatives. We have shown previously that insertion of these fluorescent protein constructs into the chromosome does not substantially influence growth rate or other biofilm-associated phenotypes (19, 37).

In preliminary experiments, CVD112 and N16961 were inoculated into separate microfluidic devices and perfused with M9 minimal media containing 0.5% glucose. After 24 h, confocal imaging revealed dramatic differences in the biofilm architecture of the two strains (Fig. 1). Consistent with prior reports, N16961 grew in well-separated microcolonies of cells about 2 μm long, with each hemispherical biofilm microcolony appearing to descend from one progenitor on the glass surface (Fig. 1*A*) (30, 37, 38). In contrast, CVD112 formed large groups of filamented cells entangled with one another (Fig. 1*B*).

We found that CVD112 filamentation occurs most strongly under nutrient-limited medium environments, as CVD112 and N16961 cells were both observed exclusively as cells ∼2 μm long when cultivated in shaken culture with nutrient-rich lysogeny broth (LB) (*SI Appendix*, Fig. S1). In other circumstances, filamentation has been associated with an acute stress response before cell death, and since CVD112 filaments were seen in M9 minimal media, but not LB, we first suspected that they might be in a disturbed physiological state. However, CVD112 showed no growth defect in either LB or M9 media relative to N16961 as measured by colony-forming unit (CFU) count (Fig. 1*C*).

In natural seawater environments, *V. cholerae* colonizes the exoskeletons of arthropods, where it secretes chitinases to digest and consume *N*-acetyl glucosamine (GlcNAc) (18). We found that CVD112, but not N16961, filaments in artificial seawater with 0.5% GlcNAc as the sole source of carbon and nitrogen, identical to the morphology shown in Fig. 1*B*. As was the case in LB and M9 media, CVD112 and N16961 growth curves are

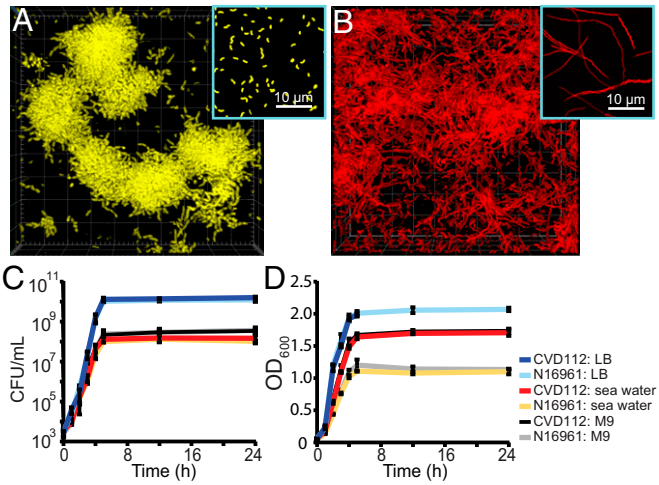

Fig. 1. Cell morphology and biofilm structures of *V. cholerae* N16961 and CVD112. (*A*) Cell-cluster biofilms of O1 El Tor strain N16961 [3D render is 80 × 80 × 15 μm length (L) × width (W) × depth (D), planktonic cells, *Inset*]. (*B*) Filamented biofilms of O139 strain CVD112 [3D render is 80 × 80 × 50 μm (L × W × D), planktonic cells, *Inset*]. Biofilm images in *A* and *B* were captured in glass-bottom chambers containing M9 minimal media with 0.5% glucose. (*C* and *D*) Growth kinetics of CVD112 and N16961 in LB, artificial seawater with 0.5% GlcNAc, and M9 minimal media with 0.5% glucose, as measured by (*C*) colony-forming unit count and (*D*) optical density at 600 nm (for each growth curve and condition, $n = 3$ biological replicates, each with three technical replicates). Error bars denote the SEM.

indistinguishable by CFU count in artificial seawater with GlcNAc, indicating similar rates of cell division (Fig. 1*C*). Following this observation, we suspected that CVD112 produces more total biomass than N16961 per unit time in low-nutrient media (where CVD112 produces filaments, while N16961 produces cells of normal length) but not in high-nutrient media (where both strains produce cells of normal length). We tested this possibility by measuring the rate of total biomass production in liquid culture by optical density instead of CFU count. As predicted, CVD112 produces biomass more quickly and to higher final density than N16961 in M9 media with glucose, and in artificial seawater with GlcNAc, but not in LB (Fig. 1*D*). This result was further confirmed with dry biomass measurements of each strain after reaching stationary phase (*SI Appendix*, Fig. S2). We visualized cells at regular time intervals over the course of their growth and confirmed that CVD112 begins filamenting in midexponential phase in seawater with GlcNAc, but not LB (*SI Appendix*, Fig. S1).

Filamentation of CVD112 in nutrient-limited conditions must derive in part from changes in cell-elongation rate relative to cell-division rate. By simultaneously staining DNA and the bacterial membrane, we found that chromosome replication continues—visible as multiple separated nucleoids—as filaments elongate (*SI Appendix*, Fig. S3). Motility assays on low-concentration agar plates (*SI Appendix*, Fig. S4), as well as direct observation by microscopy (Movie S1), showed that filamentous CVD112 cells were actively motile, though at lower speed than cells of shorter length. The relative rates of elongation and division of CVD112 can be reverted under nutrient-rich conditions, such that filamentous cells divide into multiple ∼2-μm-long cells similar to strain N16961. We could observe this directly by following the growth of CVD112 cells prefilamented in low-nutrient media, which were then transferred under an agar pad made from LB (Movie S2). From these results, we infer overall that CVD112 has a decreased rate of division, but not elongation, in low-nutrient media, which leads to filamentation in a reversible manner. As our focus will be on the biofilm ecological consequences of filamentation, we emphasize that there is no growth-related fitness defect accompanying this

morphology under the conditions tested. Beyond these observations, understanding the regulatory and mechanistic basis for filamentation, and its broader physiological relevance, are notable areas for future work.

After inspecting our set of isolates of *V. cholerae*, we found that at least one strain of O1 El Tor and O139 produces subpopulations of filamented cells on chitin in seawater, while others of each serogroup do not [*SI Appendix*, Fig. S5; *SI Appendix*, Table S2 provides a list of the differences between these strains as identified by whole-genome sequencing (39)]. Other work has noted natural variation in the propensity to filament among nontoxigenic strains of *V. cholerae* as well (40). Filamentation is thus observed in a variety of strain backgrounds and is not specific to toxigenic strains, or to one serogroup among pandemic isolates. This is the pattern one would expect to see if natural selection for filamentation varies with local environmental conditions. To understand potential reasons why this morphotype could be maintained by selection, we next set out to determine how filamentous cells interact and compete with those of shorter length in a naturalistic context.

Filamentation Promotes Colonization of Chitin Particles and Enables Matrix-Independent Biofilm Formation. We next explored the biofilm morphologies of filamenting CVD112 and nonfilamenting N16961 *V. cholerae*, simulating the natural conditions they experience in marine environments. We inoculated these strains in microfluidic channels containing PDMS traps to immobilize chitin particles (in this case, shrimp shell), a natural substrate of *V. cholerae* for biofilm growth and nutrient consumption (41, 42) (*SI Appendix*, *Materials and Methods*). The chambers were perfused with artificial seawater at a flow rate similar to what would be experienced by a descending marine snow particle (19). Other carbon and nitrogen sources were omitted from the liquid medium, in order to minimize growth in areas of the chamber other than the chitin particles.

In the process of inoculating chitin with *V. cholerae* under flow, we noticed that CVD112 filaments were particularly adept at colonizing shrimp shell surface, with single cells often wound around the contours of individual chitin particles (*SI Appendix*, Fig. S6). This suggests that single filaments can undergo large deformation in shear flow, despite the stiffness of the cell wall, and that these flexible filaments can therefore wrap around objects in the flow path. To determine if these properties give CVD112 a colonization advantage on chitin, we measured the attachment rates of filamentous CVD112 and nonfilamenting N16961 by flowing a 1:1 mixture of the two strains (normalized by total biomass per volume) onto chitin particles in artificial seawater. Filamentous *V. cholerae* does indeed colonize chitin more rapidly than short cells (Fig. 2*A*). This result holds when the two strains' colonization rates are tested in monoculture

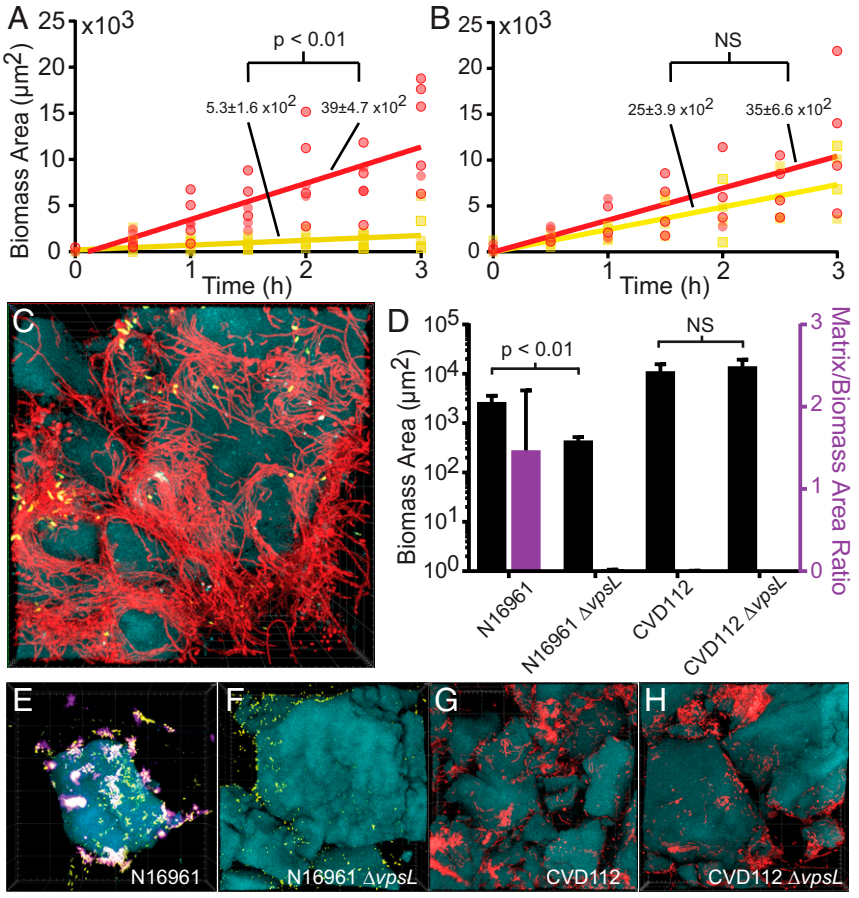

Fig. 2. Filamentous *V. cholerae* CVD112 has an increased chitin colonization rate and produces VPS- and RbmA-independent biofilms on chitin in seawater. (*A*) The rates of CVD112 (red data) and N16961 (yellow data) accumulation onto fresh chitin particles in artificial seawater ($n = 6$ biological replicates). (*B*) As in *A*, but here N16961 was pretreated for 60 min with cefalexin, which causes it to filament in a manner similar to CVD112 without reducing cell viability ($n = 4$ biological replicates). NS, not significant. (*C*) CVD112 cells (red) and N16961 (yellow) bound to pieces of chitin (blue) in artificial seawater [3D render is 85 × 85 × 60 μm (L × W × D)]. (*D*) Mean biomass production (black bars, left vertical axis) and matrix normalized to biomass (purple bar, right vertical axis) for wild type and matrix-deficient Δ*vpsL* derivatives of CVD112 and N16961 ($n = 5$ biological replicates). Error bars denote the SEM. (*E–H*) Wild-type N16961 (*E*) (yellow), N16961 Δ*vpsL* (*F*) (yellow), CVD112 (*G*) (red), and CVD112 Δ*vpsL* (*H*) (red) on chitin (blue) in seawater. Matrix stain (Cy3-conjugated antibody to RbmA-FLAG) is shown in purple [3D renders in *E–H* are 175 × 175 × 40 μm (L × W × D)].

(*SI Appendix*, Fig. S7*A*), and when cells dispersing directly from previously occupied chitin particles are flowed into new chambers containing fresh chitin (*SI Appendix*, Fig. S7*B*).

Though N16961 does not produce filaments on its own, we could artificially induce this strain to do so by treating it with subinhibitory concentrations of cefalexin for 1 h, which blocks cell division with minimal impact on cell viability or other aspects of *V. cholerae* morphology (34). N16961 pretreated in this manner exhibited similar cell elongation and a chitin colonization rate statistically equivalent to that observed for CVD112 filaments (Fig. 2*B*). Below, we assess the contribution of other adhesion factors that could influence CVD112 attachment and subsequent growth on chitin.

Following colonization, CVD112 produces biofilms that differ dramatically from those of N16961; they are composed of enmeshed cell filaments and lack the typical cell–cell packing and radial orientation associated with N16961 biofilm microcolonies (Fig. 2*C*) (26, 30). The relative absence of tight cell–cell association prompted us to ask whether CVD112 was producing biofilm matrix, including *Vibrio* polysaccharide (VPS) and the adhesin RbmA, which interacts with the cell exterior and with VPS to hold neighboring cells in close proximity (24, 26, 29, 30, 37). To assess the contribution of matrix production to filamentous biofilms on chitin, we tested CVD112 and its isogenic Δ*vpsL* null mutant, which is unable to synthesize VPS or to accumulate any of the major matrix proteins (24). Biofilm production of wild-type N16961, whose structure depends on matrix secretion (24, 25, 31), and its isogenic Δ*vpsL* null mutant were also measured for comparison. All strains contained a FLAG epitope inserted at the C terminus of the native *rbmA* locus (24, 37). Fusion of a FLAG epitope to RbmA has been shown not to interfere with its function (24, 26), and allowed us to localize and quantify RbmA by immunostaining as a proxy for general matrix accumulation.

As expected, N16961 produced biofilms with abundant RbmA, while its isogenic Δ*vpsL* mutant was impaired for biofilm growth relative to the wild-type parent and showed no matrix accumulation by RbmA staining (Fig. 2 *D*–*F*). The biomass and visible biofilm architecture of CVD112 and its Δ*vpsL* null mutant, on the other hand, were equivalent, and CVD112 biofilms showed no detectable RbmA accumulation, even in areas of dense growth (Fig. 2 *D*, *G*, and *H*). Previous reports have suggested the involvement of O-antigen and capsule polysaccharide in calcium-dependent biofilms of (nonfilamentous) *V. cholerae* O139 (43), but here we observed that filamentous biofilms did not rely on these factors: Their biomass on chitin was unchanged in the absence of calcium, and in a Δ*wbfR* background, which cannot synthesize O-antigen or capsule polysaccharide (*SI Appendix*, Fig. S8).

Recent work has demonstrated an important role for competence pili in biofilm structure and clonal autoaggregation of *V. cholerae* O1 El Tor with normal cell length on chitin (44). For filamentous biofilms of CVD112 in our experimental flow conditions, a Δ*pilA* deletion mutant lacking competence pili did not differ from CVD112 in biomass accumulation (*SI Appendix*, Fig. S8). Likewise, deletion mutants (Δ*tcpA* and Δ*gbpA*, respectively) lacking toxin-coregulated pili or chitin-binding protein were no different from the parental CVD112 (*SI Appendix*, Fig. S8). An immotile mutant (Δ*flaA*) lacking the polar flagellum showed a small but statistically significant defect in biomass accumulation, consistent with a role for the flagellum in surface colonization or exploration (25, 45, 46). On the other hand, chitin attachment and subsequent biofilm growth were highly dependent on MSHA pili (18, 46, 47), as a Δ*mshA* deletion mutant was severely defective for biomass accumulation relative to the parental CVD112 (*SI Appendix*, Fig. S8). Importantly, quantitative RT-PCR analysis of *mshA* transcripts per unit biomass indicated lower expression of *mshA* in CVD112 than in N16961 (*SI Appendix*, Fig. S9), so differential production of MSHA adhesin on its own cannot explain the augmented colonization ability of filamentous CVD112.

Overall, these results suggest that filamentation, in conjunction with other key adhesion factors including MSHA pili, yields an advantage in chitin attachment and early-stage biofilm accumulation in *V. cholerae* CVD112 relative to N16961. The filamentous biofilm structures of CVD112 are independent of the primary matrix polysaccharide VPS and cell–cell adhesin RbmA. We infer from our matrix staining and deletion mutant analysis that filamentous biofilm architecture derives at least in part from entanglement of the cells themselves, which serve as both the actively growing biomass and a foundation of the biofilm's structure.

Filamentation Is Advantageous in Frequently Disturbed Environments. Once we had found that filamentation provides an advantage during chitin attachment, we sought to understand the relative fitness effects of this cell morphology on chitin in coculture with cells of normal length that produce biofilm matrix. To do this, we inoculated CVD112 and N16961 together on chitin in artificial seawater and measured their subsequent biofilm compositions by confocal microscopy daily for 12 d. Our goal in the following experiments was to identify when and how filamentation might provide a fitness advantage relative to conventional biofilm architecture in conditions closely mimicking the marine environment *V. cholerae* naturally occupies.

When biofilms were left unperturbed for the full duration of the experiment, filamenting CVD112 cells had an initial advantage consistent with our colonization and growth rate experiments, but nonfilamenting N16961 eventually increased in frequency to become the overwhelming majority of the population (Fig. 3 *A* and *C*). Time series of single locations on the chitin surface show the progressive displacement of filamentous CVD112 biofilms by the matrix-replete biofilms of N16961 (*SI Appendix*, Fig. S10). As noted above, filamentous CVD112 biofilms are independent of VPS and RbmA matrix components, while N16961 secretes copious extracellular matrix within chitin-bound biofilms. Though CVD112 is superior in its initial surface occupation, its eventual displacement by N16961 is consistent with our prior work demonstrating that matrix secretion and cell–cell packing confer a pronounced local competitive advantage within biofilms of *V. cholerae*, as well as resistance to spatial invasion by other bacteria (13, 14, 37, 48, 49). As opposed to matrix-replete biofilms of *V. cholerae*, biofilms of filamentous CVD112 permit competing strains to invade their interior volume: They do not maintain a grip over the space they initially claim during the colonization and early growth phases of the experiment. Direct proximity to chitin is a crucial determinant of fitness in this simulated marine environment, as chitin surfaces are the sole source of carbon and nitrogen, and active flow causes any excess chitin digestion products to be swept out of the system before they can be exploited by cells at a distance from the chitin particles (19).

Although matrix-producing N16961 outcompetes CVD112 within a patch of chitin-attached biofilm over time, the latter's colonization advantage led us to speculate that it could be successful when residence times on a given chitin particle are shorter. This could be the case, for example, under frequently agitated water column conditions or when chitin particle sizes are smaller, such that they are depleted quickly. To assess this idea, we repeated our competition experiments, but instead of tracking biofilm growth within a single microfluidic chamber over 12 d, we periodically used the liquid effluent exiting the chitin chamber to inoculate a new chamber containing fresh chitin, where a new competition would resume (*SI Appendix*, Fig. S11). This process simulates a disturbance event in which dispersal increases representation on new chitin particles elsewhere in the water column. We implemented two disturbance regimes, recolonizing fresh chitin chambers once every 72 h, or once every 24 h.

When dispersed cells were taken from the effluent and allowed to recolonize fresh chitin every 72 h, filamenting CVD112 cells showed a protracted early increase in frequency, but once again were eventually outcompeted by matrix-secreting, nonfilamented N16961 cells (Fig. 3 *A*, *B*, and *D*). However, when effluent collection and recolonization of fresh chitin occurred every 24 h, the CVD112 strain dominated cocultures for the full duration of the 12-d experiment (Fig. 3 *A*, *B*, and *E*). The

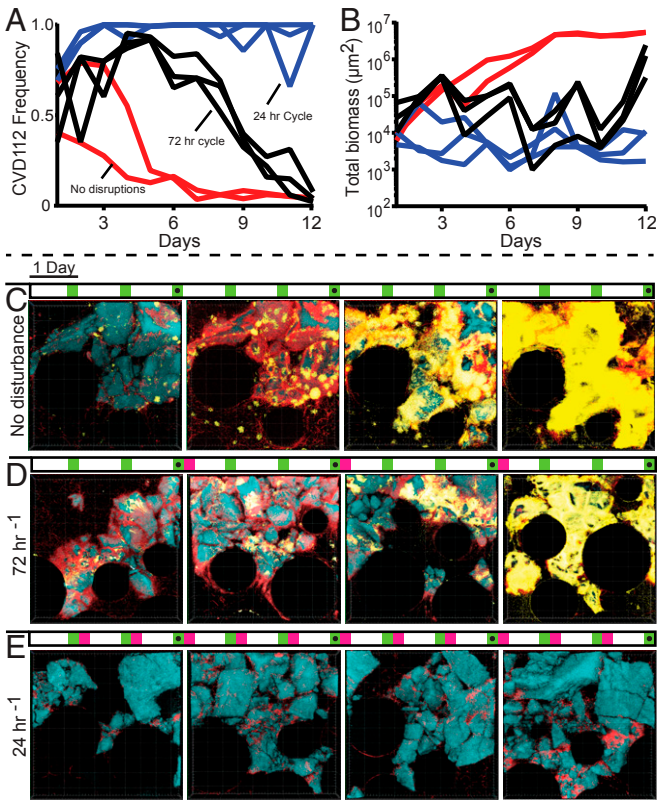

Fig. 3. Competition between short-cell N16961 (yellow) and filamenting CVD112 (red) on chitin (blue) in seawater. The two strains were grown together with different disturbance/recolonization regimes for 12 d. *A* shows the frequency (fraction of total biomass) of CVD112, while *B* shows the total biomass in the chambers for each disturbance condition. Chambers were either undisturbed (red traces in *A* and *B*; images in *C*), disrupted and reinoculated into new chitin chambers once per 72 h (black traces in *A* and *B*; images in *D*), or disrupted and reinoculated into chambers every 24 h (blue traces in *A* and *B*; images in *E*). Above each image series the treatment regime is shown with imaging times marked in green (representative images noted with black dots) and disturbance/recolonization events shown in magenta. All 3D renders in *C*–*E* are 385 × 385 × 32 μm (L × W × D).

trajectories of these population dynamics were remarkably consistent from one run of the experiment to the next in all dispersal/recolonization regimes, despite variation in one replicate to the next in the particular arrangement of chitin particles in the chamber and the locations of initial attachment by the two strains. This demonstrates the dominating strength of the effects of competition during colonization, biofilm growth, and dispersal, relative to the influence of stochastic factors such as orientation of chitin particles in the chambers, initial strain colonization patterns, or local variation in flow regime.

Discussion

Individual cell morphology varies widely within and across bacterial species (50, 51), but in most cases it is not clear how cell shape relates to emergent structure and ecology of cell collectives such as biofilms. Here we have found that some isolates of *V. cholerae* produce long cell filaments under nutrient-limited media, including conditions closely matched to the natural marine environment. This cell morphology generates a pronounced advantage in chitin surface colonization and a matrix-independent biofilm architecture that permits rapid surface occupation and high dispersal rates. However, this advantage comes at a cost: Filamentous biofilms are ultimately displaced by matrix-secreting strains in long-term competition experiments. Filamentation is thus advantageous when patches of chitin turn over quickly, such that faster colonization and reversible attachment are more important. Our results demonstrate that the shape of *V. cholerae* variants can tune the relative investment into surface colonization, long-term biofilm robustness, and dispersal back into the planktonic phase. These are fundamental elements of fitness for any biofilm-producing microbe (13, 52), and they are especially important for the marine ecology of *V. cholerae* as it colonizes, consumes, disperses from, and then recolonizes chitin in its marine environment.

Bacterial cell shape can serve a broad range of adaptive functions (49–51). The curved shape of *Caulobacter crescentus*, for example, promotes the formation of biofilms as hydrodynamic forces reorient single cells to optimize daughter cell attachment (53); this process also nucleates clonal clusters under strong flow (54, 55). Simulations and experiments with engineered variants of *Escherichia coli* suggest that rod-shaped bacteria can obtain a competitive advantage over spherical cells in colonies on agar plates, because rod-shaped cells burrow underneath spherical cells and spread more effectively to access fresh nutrients on the colony periphery (56). Filamentation has been observed in a wide variety of bacteria and eukaryotic microbes; this morphology is implicated in assisting spatial spread through soil or host tissue and defense against phagocytosing amoeboid predators (50, 57, 58). In this work, we have shown that filamentation can alter surface colonization, biofilm architecture, and, as a result, the relative investment into rapid surface occupation versus long-term competitive success in biofilms.

The biophysical bases of our results are a topic of future work, but here we note that single filaments of *V. cholerae* can rapidly bend in shear flow, despite the stiffness of the bacterial cell wall (59). Our results demonstrate that sufficiently long bacteria can behave as elastic filaments (60). In analogy with the stretching behavior of polymers in flows that approach and split at the interface with an obstacle (i.e., extensional flows), we expect that filamentous bacteria experience shear that stretches them into alignment with stationary surfaces in the flow path (61–63). This phenomenon presumably increases the dwell time and contact area of filaments in proximity to obstacles in flow (*SI Appendix*, Fig. S12). We speculate that this process, in conjunction with previously known surface-adhesion mechanisms such as MSHA pili (46, 47), promotes rapid attachment and wrapping of filaments around chitin particles (*SI Appendix*, Fig. S6).

Following surface attachment, filamentation allows the construction of biofilms in which cell–cell contacts generate a mesh network that is not dependent on the major polysaccharide or cell–cell adhesion components of the *V. cholerae* biofilm matrix. In this respect, filamentous biofilms may be analogous to a polymeric gel in which elongated cell bodies are directly associated through physical entanglement (64). Here, this cell network is more natively inclined to fast surface spreading and subsequent dispersal but also porous and prone to physical invasion by competing strains or species (*SI Appendix*, Fig. S10). This strategy of rapid colonization and biomass accumulation but high reversibility of surface association is particularly well suited to fluctuating environments in which resource patches are short-lived. This could be the case when particles are small and quickly consumed, or when disturbance events are common and destroy or disrupt particles with high frequency.

Understanding the transitions between individual cell behavior and collective properties that emerge among biofilm-dwelling bacteria is a topic of increasingly intense interest in the microbiology community. Our results here suggest that changes in cell shape are a fundamental element of this individual-to-collective transition. For *V. cholerae*, and potentially other microbes producing biofilms on and dispersing from particle to particle, filamentation may offer a surface-occupation strategy better suited to transient environments by shifting a biofilm's ability to spread over surfaces, at the expense of long-term competitive ability against matrix-replete, more highly adhesive cell groups. The ecological scope and impact of this cell morphology for *V. cholerae* and its relatives in realistic multispecies communities remain open questions for future work.

Materials and Methods

Methods for microfluidic device assembly, biological experiments, microscopy, image analysis, and statistical analysis can be found further described in *SI Appendix, Materials and Methods*.

ACKNOWLEDGMENTS. We thank Rob McClung, Mary Lou Guerinot, Daniel Schultz, Ryan Calsbeek, Deborah Hogan, George O'Toole, Melanie Blokesch, and Fitnat Yildiz for helpful comments on earlier versions of this manuscript, and Knut Drescher, Matthew Bond, and Swetha Kasetty for comments on the project. B.R.W. is supported by a GANN Fellowship from Dartmouth College. K.P. acknowledges funding by the DFG (Collaborative Research Centre TRR 174). A.P. is supported by the Swiss National Science Foundation (Project Grant 31003A_169377) and the Gabriella Giorgi-Cavaglieri Foundation. C.D.N. is supported by the National Science Foundation (MCB 1817342), a Burke Award from Dartmouth College, a pilot award from the Cystic Fibrosis Foundation (STANTO15RO), and NIH Grant P20-GM113132 to the Dartmouth BioMT COBRE.

1. H.-C. Flemming *et al*., Biofilms: An emergent form of bacterial life. *Nat. Rev. Microbiol.* **14**, 563–575 (2016).
2. T. Rudrappa, M. L. Biedrzycki, H. P. Bais, Causes and consequences of plant-associated biofilms. *FEMS Microbiol. Ecol.* **64**, 153–166 (2008).
3. O. Ciofu, C. R. Hansen, N. Høiby, Respiratory bacterial infections in cystic fibrosis. *Curr. Opin. Pulm. Med.* **19**, 251–258 (2013).
4. R. Wolcott, Disrupting the biofilm matrix improves wound healing outcomes. *J. Wound Care* **24**, 366–371 (2015).
5. R. J. Barnes *et al*., Nitric oxide treatment for the control of reverse osmosis membrane biofouling. *Appl. Environ. Microbiol.* **81**, 2515–2524 (2015).
6. K. L. Cottingham, D. A. Chiavelli, R. K. Taylor, Environmental microbe and human pathogen: The ecology and microbiology of *Vibrio cholerae*. *Front. Ecol. Environ.* **1**, 80–86 (2003).
7. H. Dang, C. R. Lovell, Microbial surface colonization and biofilm development in marine environments. *Microbiol. Mol. Biol. Rev.* **80**, 91–138 (2015).
8. M. S. Datta, E. Sliwerska, J. Gore, M. F. Polz, O. X. Cordero, Microbial interactions lead to rapid micro-scale successions on model marine particles. *Nat. Commun.* **7**, 11965 (2016).
9. T. N. Enke, G. E. Leventhal, M. Metzger, J. T. Saavedra, O. X. Cordero, Microscale ecology regulates particulate organic matter turnover in model marine microbial communities. *Nat. Commun.* **9**, 2743 (2018).
10. G. E. Leventhal *et al*., Strain-level diversity drives alternative community types in millimetre-scale granular biofilms. *Nat. Microbiol.* **3**, 1295–1303 (2018).
11. T.-F. C. Mah, G. A. O'Toole, Mechanisms of biofilm resistance to antimicrobial agents. *Trends Microbiol.* **9**, 34–39 (2001).
12. C. D. Nadell, J. B. Xavier, K. R. Foster, The sociobiology of biofilms. *FEMS Microbiol. Rev.* **33**, 206–224 (2009).
13. C. D. Nadell, B. L. Bassler, A fitness trade-off between local competition and dispersal in *Vibrio cholerae* biofilms. *Proc. Natl. Acad. Sci. U.S.A.* **108**, 14181–14185 (2011).
14. J. Yan, C. D. Nadell, B. L. Bassler, Environmental fluctuation governs selection for plasticity in biofilm production. *ISME J.* **11**, 1569–1577 (2017).
15. Y. Yawata *et al*., Competition-dispersal tradeoff ecologically differentiates recently speciated marine bacterioplankton populations. *Proc. Natl. Acad. Sci. U.S.A.* **111**, 5622–5627 (2014).
16. S. M. Faruque *et al*., Transmissibility of cholera: In vivo-formed biofilms and their relationship to infectivity and persistence in the environment. *Proc. Natl. Acad. Sci. U.S.A.* **103**, 6350–6355 (2006).
17. C. A. Hayes, T. N. Dalia, A. B. Dalia, Systematic genetic dissection of chitin degradation and uptake in *Vibrio cholerae*. *Environ. Microbiol.* **19**, 4154–4163 (2017).
18. K. L. Meibom *et al*., The *Vibrio cholerae* chitin utilization program. *Proc. Natl. Acad. Sci. U.S.A.* **101**, 2524–2529 (2004).
19. K. Drescher, C. D. Nadell, H. A. Stone, N. S. Wingreen, B. L. Bassler, Solutions to the public goods dilemma in bacterial biofilms. *Curr. Biol.* **24**, 50–55 (2014).
20. K. L. Meibom, M. Blokesch, N. A. Dolganov, C. Y. Wu, G. K. Schoolnik, Chitin induces natural competence in *Vibrio cholerae*. *Science* **310**, 1824–1827 (2005).
21. C. Lutz, M. Erken, P. Noorian, S. Sun, D. McDougald, Environmental reservoirs and mechanisms of persistence of *Vibrio cholerae*. *Front. Microbiol.* **4**, 375 (2013).
22. S. Borgeaud, L. C. Metzger, T. Scrignari, M. Blokesch, The type VI secretion system of *Vibrio cholerae* fosters horizontal gene transfer. *Science* **347**, 63–67 (2015).
23. M. Blokesch, G. K. Schoolnik, Serogroup conversion of *Vibrio cholerae* in aquatic reservoirs. *PLoS Pathog.* **3**, e81 (2007).
24. V. Berk *et al*., Molecular architecture and assembly principles of *Vibrio cholerae* biofilms. *Science* **337**, 236–239 (2012).
25. J. K. Teschler *et al*., Living in the matrix: Assembly and control of *Vibrio cholerae* biofilms. *Nat. Rev. Microbiol.* **13**, 255–268 (2015).
26. J. C. Fong *et al*., Structural dynamics of RbmA governs plasticity of *Vibrio cholerae* biofilms. *eLife* **6**, e26163 (2017).
27. C. Absalon, K. Van Dellen, P. I. Watnick, A communal bacterial adhesin anchors biofilm and bystander cells to surfaces. *PLoS Pathog.* **7**, e1002210 (2011).
28. M. Maestre-Reyna, W.-J. Wu, A. H. J. Wang, Structural insights into RbmA, a biofilm scaffolding protein of *V. cholerae*. *PLoS One* **8**, e82458 (2013).
29. K. M. Giglio, J. C. Fong, F. H. Yildiz, H. Sondermann, Structural basis for biofilm formation via the *Vibrio cholerae* matrix protein RbmA. *J. Bacteriol.* **195**, 3277–3286 (2013).
30. K. Drescher *et al*., Architectural transitions in *Vibrio cholerae* biofilms at single-cell resolution. *Proc. Natl. Acad. Sci. U.S.A.* **113**, E2066–E2072 (2016).
31. J. Yan, A. G. Sharo, H. A. Stone, N. S. Wingreen, B. L. Bassler, *Vibrio cholerae* biofilm growth program and architecture revealed by single-cell live imaging. *Proc. Natl. Acad. Sci. U.S.A.* **113**, E5337–E5343 (2016).
32. R. Hartmann *et al*., Emergence of three-dimensional order and structure in growing biofilms. *Nat. Phys.* **15**, 251–256 (2019).
33. S. Cooper, Helical growth and the curved shape of *Vibrio cholerae*. *FEMS Microbiol. Lett.* **198**, 123–124 (2001).
34. T. M. Bartlett *et al*., A periplasmic polymer curves *Vibrio cholerae* and promotes pathogenesis. *Cell* **168**, 172–185.e15 (2017).
35. T. Dörr, F. Cava, H. Lam, B. M. Davis, M. K. Waldor, Substrate specificity of an elongation-specific peptidoglycan endopeptidase and its implications for cell wall architecture and growth of *Vibrio cholerae*. *Mol. Microbiol.* **89**, 949–962 (2013).
36. C. O. Tacket *et al*., Initial clinical studies of CVD 112 *Vibrio cholerae* O139 live oral vaccine: Safety and efficacy against experimental challenge. *J. Infect. Dis.* **172**, 883–886 (1995).
37. C. D. Nadell, K. Drescher, N. S. Wingreen, B. L. Bassler, Extracellular matrix structure governs invasion resistance in bacterial biofilms. *ISME J.* **9**, 1700–1709 (2015).
38. C. D. Nadell *et al*., Cutting through the complexity of cell collectives. *Proc. Biol. Sci.* **280**, 20122770 (2013).
39. R. W. Wucher *et al*., Vibrio cholerae filamentation promotes chitin surface attachment at the expense of competition in biofilms. European Nucleotide Archive. https://www.ebi.ac.uk/ena/data/view/PRJEB32555. Deposited 15 May 2019.
40. F. Hassan, M. Kamruzzaman, J. J. Mekalanos, S. M. Faruque, Satellite phage TLCφ enables toxigenic conversion by CTX phage through dif site alteration. *Nature* **467**, 982–985 (2010).
41. J. Reidl, K. E. Klose, *Vibrio cholerae* and cholera: Out of the water and into the host. *FEMS Microbiol. Rev.* **26**, 125–139 (2002).
42. R. Stocker, J. R. Seymour, Ecology and physics of bacterial chemotaxis in the ocean. *Microbiol. Mol. Biol. Rev.* **76**, 792–812 (2012).
43. K. Kierek, P. I. Watnick, The *Vibrio cholerae* O139 O-antigen polysaccharide is essential for Ca^{2+}-dependent biofilm development in sea water. *Proc. Natl. Acad. Sci. U.S.A.* **100**, 14357–14362 (2003).
44. D. W. Adams, S. Stutzmann, C. Stoudmann, M. Blokesch, DNA-uptake pili of *Vibrio cholerae* are required for chitin colonization and capable of kin recognition via sequence-specific self-interaction. *Nat. Microbiol.* 10.1038/s41564-019-0479-5 (2019).
45. F. H. Yildiz, K. L. Visick, *Vibrio* biofilms: So much the same yet so different. *Trends Microbiol.* **17**, 109–118 (2009).
46. C. J. Jones *et al*., C-di-GMP regulates motile to sessile transition by modulating MshA pili biogenesis and near-surface motility behavior in *Vibrio cholerae*. *PLoS Pathog.* **11**, e1005068 (2015).
47. A. S. Utada *et al*., *Vibrio cholerae* use pili and flagella synergistically to effect motility switching and conditional surface attachment. *Nat. Commun.* **5**, 4913 (2014).
48. J. Schluter, C. D. Nadell, B. L. Bassler, K. R. Foster, Adhesion as a weapon in microbial competition. *ISME J.* **9**, 139–149 (2015).
49. A. Persat *et al*., The mechanical world of bacteria. *Cell* **161**, 988–997 (2015).
50. D. C. Yang, K. M. Blair, N. R. Salama, Staying in shape: The impact of cell shape on bacterial survival in diverse environments. *Microbiol. Mol. Biol. Rev.* **80**, 187–203 (2016).
51. K. D. Young, The selective value of bacterial shape. *Microbiol. Mol. Biol. Rev.* **70**, 660–703 (2006).
52. P. K. Singh *et al*., *Vibrio cholerae* combines individual and collective sensing to trigger biofilm dispersal. *Curr. Biol.* **27**, 3359–3366.e7 (2017).
53. A. Persat, H. A. Stone, Z. Gitai, The curved shape of *Caulobacter crescentus* enhances surface colonization in flow. *Nat. Commun.* **5**, 3824 (2014).
54. T. Rossy, C. D. Nadell, A. Persat, Cellular advective-diffusion drives the emergence of bacterial surface colonization patterns and heterogeneity. *Nat. Commun.* **10**, 2471 (2019).
55. R. Martínez-García, C. D. Nadell, R. Hartmann, K. Drescher, J. A. Bonachela, Cell adhesion and fluid flow jointly initiate genotype spatial distribution in biofilms. *PLoS Comput. Biol.* **14**, e1006094 (2018).
56. W. P. J. Smith *et al*., Cell morphology drives spatial patterning in microbial communities. *Proc. Natl. Acad. Sci. U.S.A.* **114**, E280–E286 (2017).
57. J. Möller, T. Luehmann, H. Hall, V. Vogel, The race to the pole: How high-aspect ratio shape and heterogeneous environments limit phagocytosis of filamentous *Escherichia coli* bacteria by macrophages. *Nano Lett.* **12**, 2901–2905 (2012).
58. D. J. Horvath , Jr *et al*., Morphological plasticity promotes resistance to phagocyte killing of uropathogenic *Escherichia coli*. *Microbes Infect.* **13**, 426–437 (2011).
59. Y. Deng, M. Sun, J. W. Shaevitz, Direct measurement of cell wall stress stiffening and turgor pressure in live bacterial cells. *Phys. Rev. Lett.* **107**, 158101 (2011).
60. P. A. de Boer, R. E. Crossley, L. I. Rothfield, Central role for the *Escherichia coli* minC gene product in two different cell division-inhibition systems. *Proc. Natl. Acad. Sci. U.S.A.* **87**, 1129–1133 (1990).
61. D. E. Smith, H. P. Babcock, S. Chu, Single-polymer dynamics in steady shear flow. *Science* **283**, 1724–1727 (1999).
62. T. T. Perkins, D. E. Smith, S. Chu, Single polymer dynamics in an elongational flow. *Science* **276**, 2016–2021 (1997).
63. D. Kawale *et al*., Polymer conformation during flow in porous media. *Soft Matter* **13**, 8745–8755 (2017).
64. W. W. Graessley, *The Entanglement Concept in Polymer Rheology* (Advances in Polymer Science, Springer, Berlin, 2006), vol. 16.